AIChE

Subgrid Scale Scalar Variance in High-Schmidt-Number Turbulence

Ryoichi Kurose and Naohisa Takagaki
Dept. of Mechanical Engineering and Science, Advanced Research Institute of Fluid Science and Engineering, Kyoto University, Yoshida-Honmachi, Sakyo-ku, Kyoto-shi, Kyoto 606-8501, Japan

Takenobu Michioka
Environmental Science Research Laboratory, Central Research Institute of Electric Power Industry (CRIEPI), 1646 Abiko, Abiko-shi, Chiba 270-1194, Japan

Naoki Kohno and Satoru Komori
Dept. of Mechanical Engineering and Science, Advanced Research Institute of Fluid Science and Engineering, Kyoto University, Yoshida-Honmachi, Sakyo-ku, Kyoto-shi, Kyoto 606-8501, Japan

DOI 10.1002/aic.12591
Published online March 31, 2011 in Wiley Online Library (wileyonlinelibrary.com).

The subgrid scale (SGS) variance for a high-Schmidt-number passive scalar of Sc $>> 1$ *is measured using a high-resolution planar laser-induced fluorescence technique in a grid-generated turbulent liquid flow, and the values of the model coefficients in the scale-similarity model and the scalar-gradient model used for estimating the SGS scalar variance are experimentally evaluated. The results show that for both models, the measured values are much larger than the well-known values obtained in the previous studies done for non-high-*Sc *scalars of* Sc $\cong 1$. *Similarly, the measured value of the model coefficient in the scalar-gradient model tends to be larger than the value estimated by the dynamic procedure. The increases in the measured values of the model coefficients for the high-*Sc *scalar can be explained by the presence of the viscous-convective range showing a nearly (−1)-slope in the high-wavenumber range of the power spectrum of concentration fluctuation.* © 2011 American Institute of Chemical Engineers *AIChE J,* 58: 377–384, 2012
Keywords: turbulence, mixing, high-Scmidt-number turbulence, liquid flow, SGS scalar variance, PLIF

Introduction

Mixing and transport of passive scalars by turbulence are often encountered in many geophysical and industrial processes. It is therefore of great importance to clarify the mechanism and develop the models for numerical simulations such as large-eddy simulation (LES). In particular, it is well known that the problem becomes much more complex and difficult to be solved in the case of high-Schmidt-number scalars ($Sc >> 1$, where $Sc = \nu/D$, ν is the kinematic viscosity and D is the diffusion coefficient). This is because in turbulent flows with the high-Sc scalars, the Batchelor length scale, which is a small-scale variation of scalar, η_B ($= \eta_K/Sc^{1/2}$), is much smaller than the Kolmogorov length scale η_K. Recently, thanks to the progresses in the performances of measuring systems and computers, the number of studies on the mechanism and modeling for such high-Sc scalars in turbulent flows increases both by means of experiments[1–3] and numerical simulations.[4–11]

Correspondence concerning this article should be addressed to R. Kurose at kurose@mech.kyoto-u.ac.jp.

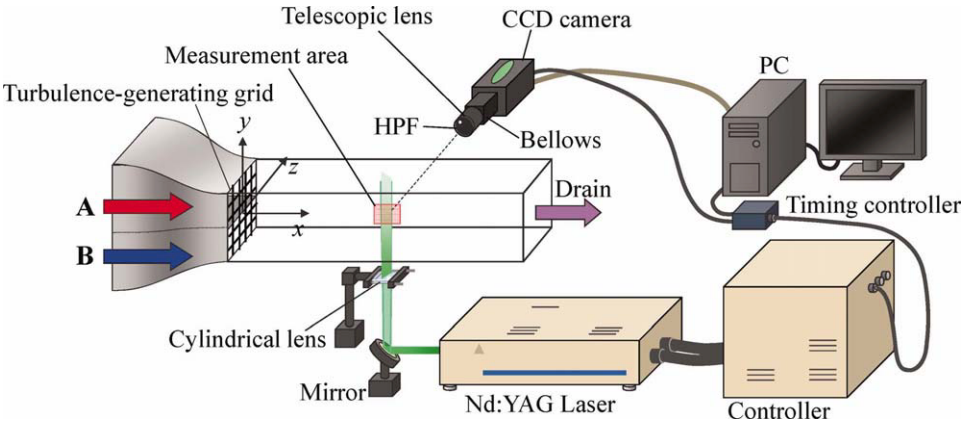

Figure 1. Schematic diagram of experimental apparatus and measuring system.

[Color figure can be viewed in the online issue, which is available at wileyonlinelibrary.com.]

One of the uncertainties is the modeling of subgrid scale (SGS) variance of nonreactive scalar, which, for example, can be an input parameter in using assumed probability density functions (PDFs) for the turbulent reaction models in LES.[12–19] The SGS scalar variance of φ, $\overline{\varphi''^2}$, is modeled by Cook and Riley[12] under a scale-similarity assumption as

$$\overline{\varphi''^2} = C_f \widetilde{\varphi''^2} \approx C_f(\widetilde{\overline{\varphi}^2} - \widetilde{\overline{\varphi}}^2), \tag{1}$$

where C_f is the model coefficient, φ'' is the fluctuation of φ (i.e., $\varphi = \overline{\varphi} + \varphi''$), and the bar and tilde denote the grid- and test-filtering values, respectively. Michioka and Komori[5] and Kurose et al.[11] applied the scale-similarity model to different turbulent reaction models (i.e., conserved scalar model, direct closure model, or flamelet model) for LES of a turbulent reacting liquid flow with high-Sc scalars ($Sc >> 1$) and validated them by comparing with the experiments.[20–23] As the results, they empirically found that the adequate value of C_f in the scale-similarity model is 5.0, which does not agree with the previous suggestion that C_f is around unity[12,24] for turbulent combusting gaseous flows with non-high-Sc scalars ($Sc \cong 1$). The reason is considered due to the difference in Schmidt number, but the validity of the value has not been fully proven, and the underling physics has not been explicitly understood yet.

The purpose of this study is therefore to experimentally evaluate not only the value of C_f but also the value of the model coefficient in another algebraic model, namely the scalar-gradient model in a same grid-generated turbulent liquid flow with a high-Sc scalar ($Sc >> 1$). The flow field is the same as in previous studies by Komori et al.[20–23] The two-dimensional behavior of the mixing and transport of the high-Sc scalar is captured by a high-resolution planar laser-induced fluorescence (PLIF) technique.

Experiments

Figure 1 shows the experimental apparatus and measuring system. The test apparatus used was a water tunnel made of polymethylemetacrylate, 1.5 m in length, and 0.1 × 0.1 m in cross-section. A turbulence-generating grid consisting of round rods was installed at the entrance to the test section. The mesh size M and the diameter of the rod d were 0.02 and 0.003 m, respectively. The flow was completely separated by a splitter plate into upper and lower streams from the reservoir tanks until the entrance to the test section. Both mean velocities of the nonpremixed upper and lower streams, U, were set to the same value of 0.25 m/s, so that a shear-free mixing layer was developed downstream of a turbulence grid. The Reynolds number based on the mesh size M and cross-sectionally averaged velocity U, Re_M, was 5000. Measurements of concentration were conducted downstream of a turbulence grid at $x/M = 15$. Fresh water without any chemical species was used as the lower stream, and an aqueous solution with Rhodamine B ($C_{28}H_{31}N_2O_3Cl$) with concentration of 1.0×10^{-4} mol/m^3 was used as the upper stream. The Schmidt number Sc of the Rhodamine B is estimated to be about 2500.[25,26]

The measurements of instantaneous concentration of Rhodamine B were made in the above mixing layer using a PLIF technique (Dantec 80N system) as shown in Figure 1. The Nd:YAG laser (wave length: $\lambda = 532$ nm; Spectra-Physics PRO270-10) was changed to a laser sheet using a cylindrical lens of 0.1-m focal length, and the laser sheet was introduced from the bottom of the test section to the measured cross-section. The intensity of the laser was 0.9 J per one pulse, and the pulse duration was 10 ns. The diameter of laser beam at the outlet of the laser head and the beam divergence were 13 mm and 0.5 mrad, respectively. The thickness of the laser sheet at the focal point calculated by geometric optics was about 50 μm. The spatial resolution of a digital CCD camera (Dantec Flow Sense 2M) with the frame rate of 10 frames per second was 1600 × 1200 pixels. A telescopic lens (Nikon AF Nikkor 85 mm 1:1.8D) and a bellows (Nikon PB-6) were attached to the CCD camera, and the imaging area and the minimum spatial resolution were 16 × 12 mm^2 and 10 μm, respectively. In addition, a high-pass optical filter was attached to the CCD camera for capturing just the fluorescence of Rhodamine B. The timing for capturing images was controlled by an external trigger signal from the controller of the Nd:YAG laser. The supplementary experiments for obtaining the linear calibration curve between the digitalized fluorescence intensity and concentration of Rhodamine B were conducted, and the fluorescence intensities in the captured raw images was normalized using the calibration curve. In the calibration, the background noise, the initial intensity distribution of the laser

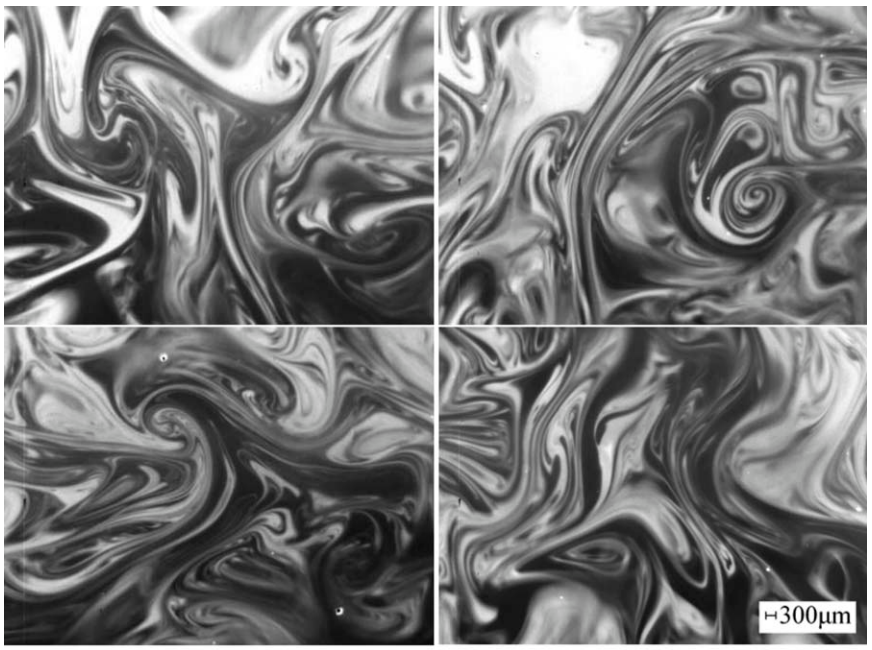

Figure 2. Typical images of instantaneous scalar concentration field.

sheet, the affects of the attenuation of the laser intensity in the water tunnel flow, and photobleaching were considered. The distortion can be negligible in the present optical setup.

Thus, the spatial and time scales of the present measuring technique were 10–50 μm and 10 ns, respectively. These resolutions are comparable or finer than those in the recent studies using similar leading-edge high-resolution PLIF techniques (see Ref. 1). On the other hand, it was estimated that the Kolmogorov and Bachelor length scales and Kolmogorov time scale, η_K, η_B, and t_K, are about 300 μm, 6 μm, and 1 ms, respectively, at $x/M = 15$.[20–23] Although the present resolutions are larger than the Bachelor scales, the contribution of scalar concentration fluctuation at such higher wavenumbers on the SGS scalar variance are negligibly small, as stated later. Therefore, they are sufficiently smaller than the Kolmogorov scales, so that it is considered that the present measuring technique has enough resolutions for investigating the general characteristics of the SGS variance for high-Sc scalars. In addition, as the thickness of the laser sheet is much smaller than the grid scales for standard LES, the discussion on the SGS scalar variance by using PLIF data is considered to be valid.

Results and Discussion

LIF image for scalar concentration

Figure 2 shows the examples of images of instantaneous scalar concentration field obtained by the PLIF technique. The size of each image is 16×12 mm^2, and the white color indicates the Rhodamine B concentration. The scalar concentration is observed to distribute in smaller scales than the Kolmogorov length scale η_K.

The energy spectra of scalar concentration fluctuation are shown for four typical images in Figure 3. Here, the energy spectra with and without a low-pass filtering operation to eliminate noise are shown. As the low-pass filter, box filter with the width of 50 μm is used. The wavenumber k is nondimensionalized by the Kolmogorov wavenumber. The wavenumbers corresponding to the Kolmogorov and Bachelor length scales are indicated by k_K (= 1.0) and k_B, respectively. Irrespective of the use of the low-pass filter, as suggested and reported in previous studies (i.e., Refs. 27 and 28), the viscous-convective range showing a nearly (−1)-slope is observed around at the Kolmogorov wavenumber of $k = k_K$. On the other hand, the inertial-convective range, which is supposed to show a (−5/3)-slope at $k < k_K$ is not observed in the figure. This is considered due to that the imaging area is too small and to fully capture the turbulent eddies larger than the integral length scale. However, Komori et al.[20,22] confirmed the presence of the inertial-convective range of (−5/3)-slope in the range of $\eta = 0.625$–10.0 mm at $x/M = 8$ in the same flow field as in this study by using a single-point LIF. It is also found that at the viscous-diffusive range of $k > k_K$, the energy spectra show marked decays and broadings toward the higher wavenumber range of $k \cong k_B$ owing to noise and that the broadings are suppressed by the low-pass filtering operation. From this figure, it can be said that the resolution limit of the present measurements is about 15–30 μm.

Model coefficient for the scale-similarity model

To evaluate C_f in Eq. 1 for LES, the values of $\overline{\varphi''^2}$ and $\widetilde{\varphi''^2}(\approx \widetilde{\overline{\varphi}^2} - \widetilde{\overline{\varphi}}^2)$ are calculated using the images obtained by the PLIF technique. Figures 4 and 5 show the joint PDF of $\overline{\varphi''^2}$ and $\widetilde{\varphi''^2}(\approx \widetilde{\overline{\varphi}^2} - \widetilde{\overline{\varphi}}^2)$ with and without the low-pass filtering operation. A dense part denotes a high PDF value, and the value gradually decreases with decreasing the thickness. Here,

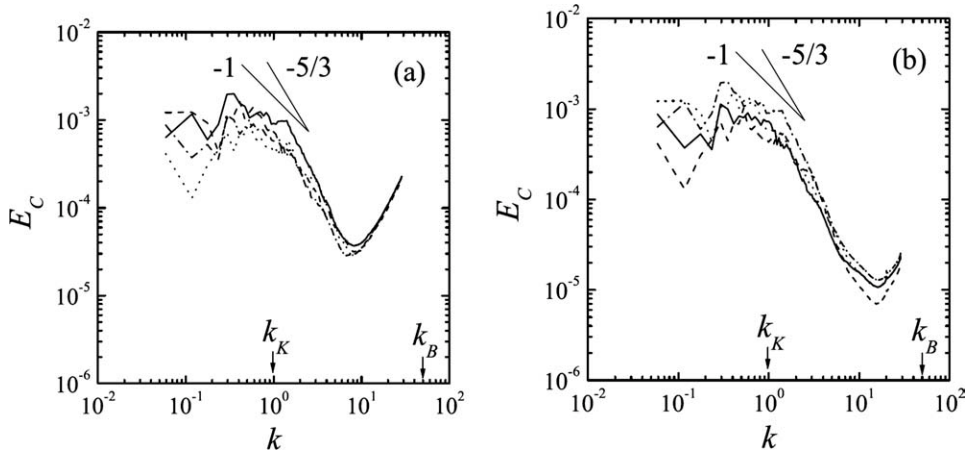

Figure 3. Typical energy spectra of scalar concentration fluctuation.

(a) Nonfiltered case; (b) filtered case.

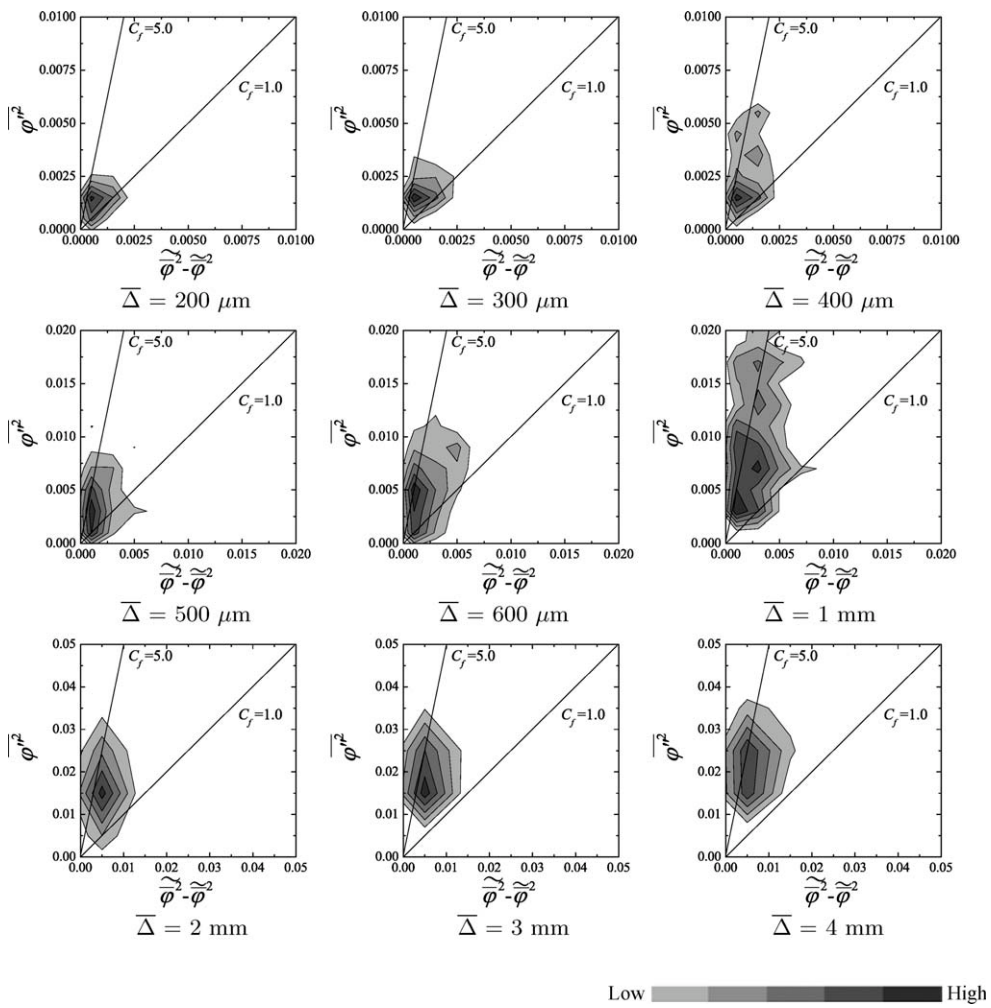

Figure 4. Joint probability density function of $\overline{\varphi''^2}$ and $\widetilde{\varphi''^2}(\approx \widetilde{\overline{\varphi}^2} - \widetilde{\overline{\varphi}}^2)$ in nonfiltered case.

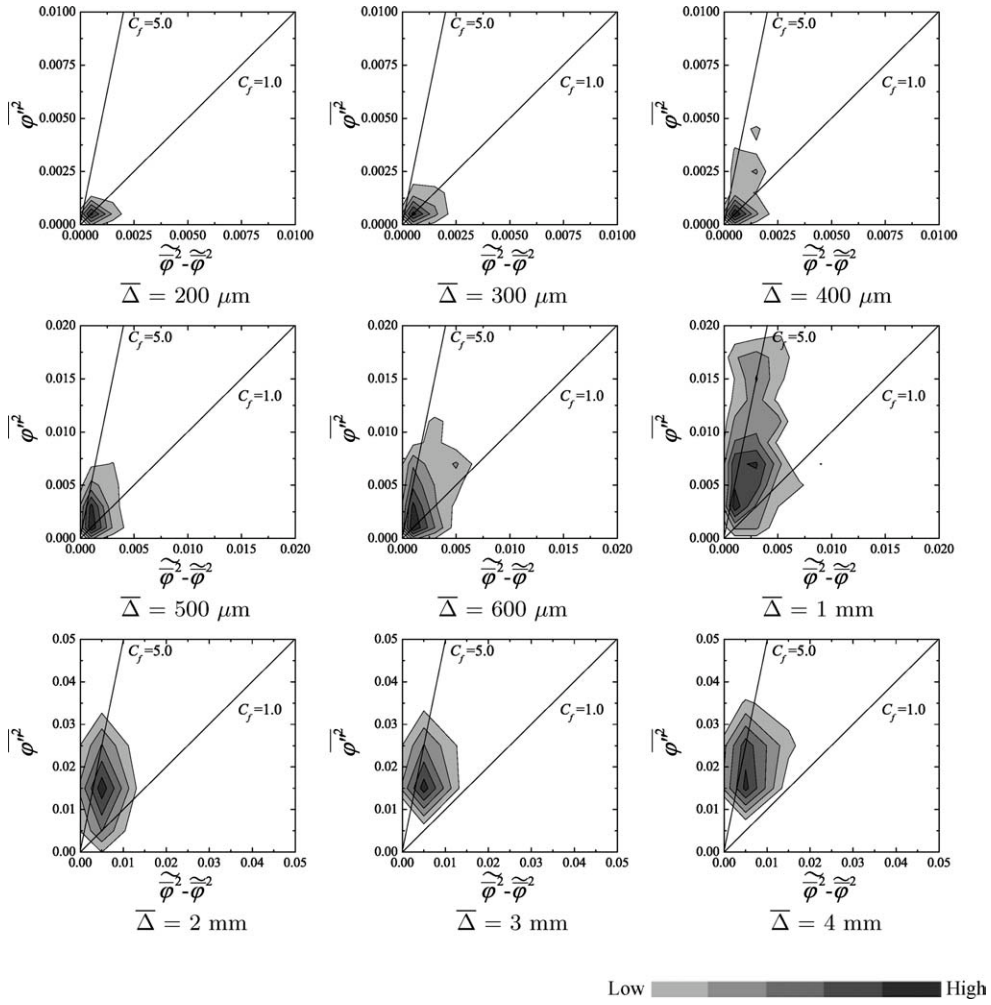

Figure 5. Joint probability density function of $\overline{\varphi''^2}$ and $\widetilde{\varphi''^2}(\approx \widetilde{\overline{\varphi}^2} - \widetilde{\overline{\varphi}}^2)$ in filtered case.

the assumed grid scale for LES, $\overline{\Delta}$, is varied from 0.2 to 4 mm and the test-filter width is set to be 2 $\overline{\Delta}$. For this analysis, 600 samples in which the Rhodamine B is well mixed at smaller scales are extracted. The slopes of $C_f = 1.0$ and 5.0 are shown in the figure. No effective difference is observed between the distributions of the PDF with and without the low-pass filtering operation. This suggests that the broadings owing to noise observed at the higher wavenumber range of $k \cong k_B$ hardly affect the value of C_f. In addition, as the box filter with the width of 50 μm is used as the low-pass filter, the coincident of the value of C_f implies that the use of the laser sheet with the thickness of 50 μm is valid for the estimation of C_f. The reason why the smaller scales than 50 μm do not affect the value of C_f very much may be explained by the finding of Wang et al.[29] that the most expected scale for the velocity field is eight times Kolmogorov length. That is, the dominant scale for the scalar variance may be much larger than the Batchelor scale. It is also found that in both cases the best-fitting slope for the PDF increases with increasing $\overline{\Delta}$ and clearly becomes $C_f = 5.0$ for $\overline{\Delta} \geq 1$ mm whose scale is in the inertial-convective range. This value of $C_f = 5.0$ completely corresponds to that obtained by the previous numerical predictions in Michioka and Komori[5] and Kurose et al.,[11] which supports the validity of $C_f = 5.0$ for high-Sc scalars. For $\overline{\Delta} \leq 1$ mm, on the other hand, the best-fitting slope for the PDF tends to gradually decrease and approach to $C_f = 1.0$.

The reason why the value of C_f for the scalar with $Sc >> 1$ becomes larger than that for the scalar with $Sc \cong 1$ (i.e., $C_f \cong 1.0$, Refs. 12 and 24) can be explained in the view of the energy spectrum. As mentioned above in Figure 3, for the high-Sc scalar, the viscous-convective range showing a nearly (-1)-slope in the power spectrum of concentration fluctuation spreads around from the Kolmogorov wavenumber of $k = k_K$ to the higher-wavenumber range. That is, the effect of the Schmidt number appears only at smaller scales than the grid scale. This phenomenon consequently increases the SGS scalar variance $\overline{\varphi_2''}$, whereas it hardly changes the test-filtered scalar variance $\widetilde{\varphi''^2}$ irrespective of the Schmidt number. As a result, C_f increases with increasing the Schmidt number. However, it should also be noted that this interpretation is valid only for the standard LES conditions in which the grid scale and the test-filter width are set to be in the inertial-convective range showing the $(-5/3)$-slope at $k < k_K$. This is because the effect of the concentration fluctuation for the high-Sc scalar in the high-wavenumber range becomes small in the cases that the grid scale and the test-filter width are in the same nearly (-1)-slope. In fact, as shown in Figures 4 and

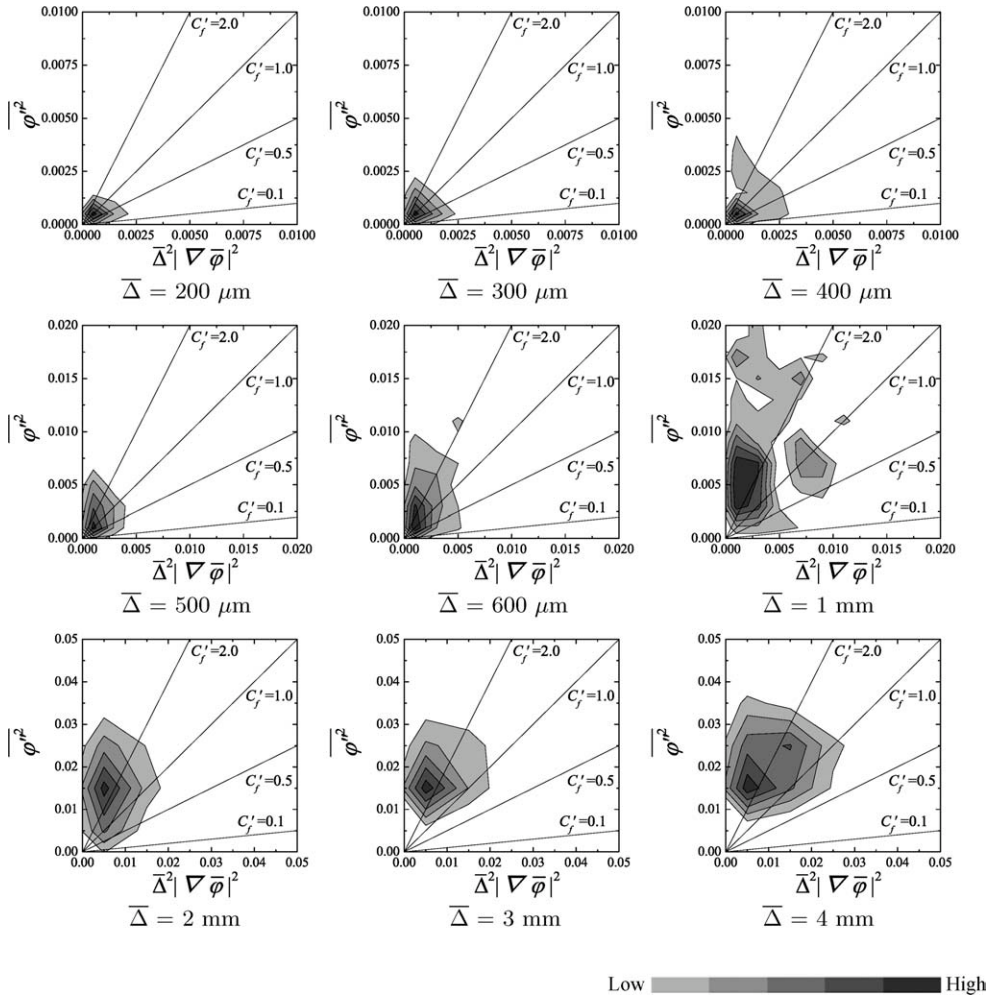

Figure 6. Joint probability density function of $\overline{\varphi''^2}$ and $\overline{\Delta}^2|\nabla\overline{\varphi}|^2$.

5, C_f decreases to around unity when the assumed grid scale is set to be smaller than the Kolmogorov scale.

Although only one high-Sc scalar is considered in this study, model coefficients in general mixing models for computations of turbulent reacting flows are considered to depend on the Schmidt number.[5,30] Michioka and Komori[5] showed by performing DNS of isotropic turbulent liquid flows with passive scalar for different Schmidt numbers of Sc = 1–600 that C_f reaches to a constant value of 5.0 for $Sc \geq 50$. The reason is speculated that the contribution of the spreading viscous-convective range to the SGS scalar variance becomes negligibly small at very high wavenumbers because the power spectrum drastically decreases in the viscous-convective range. Although the truth of this speculation has been uncertain because the resolutions of their DNS did not reach the Bachelor length scales especially in the cases of the high-Sc scalars, the present experimental results endorse the validity of the speculation.

Model coefficient for the scalar-gradient model

Instead of the scale-similarity model by Cook and Riley,[12] Pierce and Moin[13] derived another algebraic model for the SGS scalar variance on the basis of the scalar-gradient model under the assumptions of local homogeneity and local equilibrium for the SGSs as

$$\overline{\varphi''^2} = C_f'\overline{\Delta}^2|\nabla\overline{\varphi}|^2, \tag{2}$$

where the value of C'_f is determined dynamically as

$$\begin{aligned} C_f' &= \frac{\langle LM\rangle}{\langle M^2\rangle}, \\ L &= \widetilde{\overline{\varphi}^2} - \widetilde{\overline{\varphi}}\,\widetilde{\overline{\varphi}}, \\ M &= \widetilde{\overline{\Delta}}^2|\nabla\widetilde{\overline{\varphi}}|^2 - \overline{\Delta}^2\widetilde{|\nabla\overline{\varphi}|^2}, \end{aligned} \tag{3}$$

and $\overline{\Delta}$ is the local filter width. The bracket $\langle\ \rangle$ means the ensemble average. However, Kurose et al.[11] showed that compared with the scale-similarity model, this dynamic model hardly improves the accuracy of the prediction of φ''^2 in LES of a turbulent reacting liquid flows with high-Sc scalars ($Sc \cong 600$). The joint PDF of φ''^2 and $\overline{\Delta}^2|\nabla\overline{\varphi}|^2$ with the low-pass filtering operation is shown in Figure 6. The slopes of C'_f = 0.1, 0.5, 1.0, and 2.0 are shown in the figure. Similar to C_f in the scale-similarly model, the best-fitting slope for the PDF increases with increasing $\overline{\Delta}$ and becomes $C'_f = 2.0$ for $\overline{\Delta} \geq 1$ mm. For $\overline{\Delta} < 1$ mm, on the other hand, the best-fitting slope

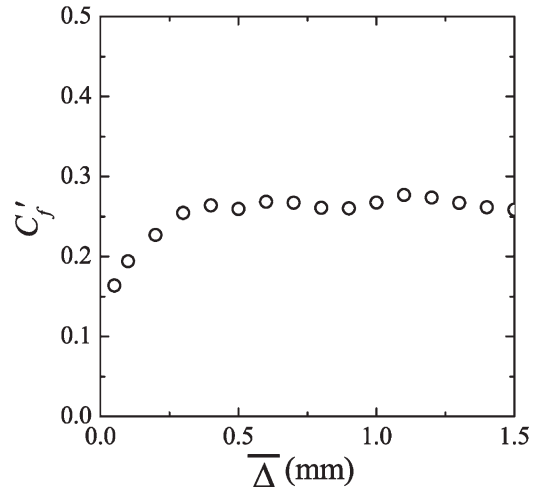

Figure 7. Relation between C'_f calculated by Eq. 3 and grid scale $\overline{\Delta}$.

for the PDF tends to gradually decrease and approach to $C'_f = 0.5$. For comparison, the value of C'_f calculated by Eq. 2 is plotted against the grid scale $\overline{\Delta}$ in Figure 7. Although C'_f increases with increasing $\overline{\Delta}$ nearly from the value predicted by Bradley and Jones[31,32] (i.e., $C'_f = 0.09$ and 0.13) and approaches to the larger value of $C'_f = 0.25$, it is still almost 10 times smaller than the value calculated by $\varphi''^2/(\overline{\Delta}^2|\nabla\overline{\varphi}|^2)$ for $\overline{\Delta} \geq 1$ mm (see Figure 6). This contrariety means that like the scale-similarity model, the scalar-gradient model cannot predict the SGS scalar variance for the high-*Sc* scalars very much, either. That is, not only the scale-similarity model with $C_f = 1.0$ but also the scalar-gradient model with the dynamic procedure tends to underestimate the SGS scalar variance for the high-*Sc* scalars. This is considered due to the fact that the increase in the Schmidt number dramatically increases the SGS scalar variance φ''^2, whereas it hardly changes the resolved scalar gradient $|\nabla\overline{\varphi}|$.

Conclusions

In terms of numerical simulations and empirical investigations, Michioka and Komori[5] first suggested that the adequate value of the model coefficient C_f in evaluating the SGS scalar variance in the scale-similarity model[11] for high-*Sc* scalars of $Sc > 1$ is much higher than those for non-high-*Sc* scalars of $Sc \cong 1$ and Kurose et al.[11] subsequently showed that the expected value not only for C_f of the scale-similarity model but also for the model coefficient C'_f of the scalar-gradient model is larger for high-*Sc* scalars than those for non-high-*Sc* scalars. To elucidate the validity of the results and the underling physics, the values of C_f and C'_f in a grid-generated turbulent liquid flow with a high-*Sc* scalar ($Sc > 1$) was measured using a high-resolution PLIF technique. It was found that the measured value of C_f in the scale-similarity model (i.e., $C_f = 5.0$) is found to be much larger than the well-known values of around unity obtained in the previous studies done for non-high-*Sc* scalars[12,24] but completely correspond to that obtained by the previous numerical prediction in Michioka and Komori[5] and Kurose et al.[11] Similarly, the measured value of the model coefficient C'_f in the scalar-gradient model (i.e., $C'_f = 2.0$) is much larger than the values obtained for non-high-*Sc* scalars both by the previous DNS[31,32] and by the dynamic procedure.[13] These facts mean that not only the scale-similarity model with $C_f = 1.0$ but also the scalar-gradient model with the dynamic procedure tends to underestimate the SGS scalar variance for the high-*Sc* scalars. The increases in the measured values of C_f and C'_f for the high-*Sc* scalars can be explained by the presence of the viscous-convective range showing a nearly (-1)-slope in the high-wavenumber range of the power spectrum of concentration fluctuation. That is, as far as the standard grid condition is provided for the LES, the increase in the Schmidt number increases the SGS scalar variance, whereas it hardly changes the resolved scalar properties. One possible option for improving the prediction of the SGS scalar variance to account for high Schmidt numbers would be to solve a transport equation for that scalar, but this would necessitate the precise evaluation of the scalar dissipation rate (e.g., Refs. 9 and 33). Unfortunately, the evaluation of the scalar dissipation rate requires much finer spatial resolution than could be achieved in this study.

Acknowledgments

The authors thank Drs. T. Kanzaki and K. Tanno of Central Research Institute of Electric Power Industry (CRIEPI) for their help in conducting the PLIF measurements. The authors are also grateful to Prof. H. Kobayashi of Keio University for his useful discussion.

Literature Cited

1. Dasi LP, Schuerg F, Webster DR. The geometric properties of high-Schmidt number passive scalar iso-surfaces in turbulent boundary layers. *J Fluid Mech*. 2007;588:253–277.
2. Nicolas JM, Schilling O, Youngs D, Andrews MJ. Measurements of molecular mixing in a high-Schmidt-number Rayleigh-Taylor mixing layer. *J Fluid Mech*. 2009;632:17–48.
3. Westerweel J, Fukushima C, Pedersen JM, Hunt JCR. Momentum and scalar transport at the turbulent/non-turbulent interface of a jet. *J Fluid Mech*. 2009;631:199–230.
4. Boguchi D, Domaradzki JA, Yeung PK. Direct numerical simulations of passive scalars with Pr > 1 advected by turbulent flow. *J Fluid Mech*. 1997;343:111–130.
5. Michioka T, Komori S. Large-eddy simulation of a turbulent reacting liquid flow. *AIChE J*. 2004;50:2705–2720.
6. Schumacher J, Sreenivasan KR, Yeung PK. Very fine structures in scalar mixing. *J Fluid Mech*. 2005;531:113–122.
7. Onishi R, Komori S. Thermally-stratified liquid turbulence with a chemical reaction. *AIChE J*. 2006;52:456–468.
8. Hickel S, Adams NA, Mansour NN. Implicit subgrid-scale modeling for large-eddy simulation of passive-scalar mixing. *Phys Fluids*. 2007;19:095102.
9. Burton GC. The nonlinear large-eddy simulation method applied to Sc = 1 and Sc > 1 passive-scalar mixing. *Phys Fluids*. 2008;20:035103.
10. Ishimoto S, Sato M, Seo S, Tanahashi M, Miyauchi T. Fine scale structure and fractal geometry of turbulent scalar mixing at high Schmidt numbers. In Proceedings of the Sixth International Symposium on Turbulence and Shear Flow Phenomena, Seoul, Korea 2009;61–66.
11. Kurose R, Michioka T, Kohno N, Baba Y, Komori S. Application of flamelet model to LES of turbulent reacting liquid flows. *AIChE J*. 2011;57:911–917.
12. Cook AW, Riley JJ. A subgrid model for equilibrium chemistry in turbulent flows. *Phys Fluids*. 1994;6:2868–2870.
13. Pierce CD, Moin PA. Dynamic model for subgrid-scale variance and dissipation rate of a conserved scalar. *Phys Fluids*. 1998;10:3041–3044.
14. Mustata R, Valiño L, Jiménez C, Jones WP, Bondi S. A probability density function Eulerian Monte Carlo field method for large eddy

simulations: application to a turbulent piloted methane/air diffusion flame (Sandia D). *Combust Flame*. 2006;145:88–104.
15. Vreman AW, Albrecht BA, van Oijena JA, de Goey LPH, Bastiaans JRM. Premixed and nonpremixed generated manifolds in large-eddy simulation of Sandia flame D and F. *Combust Flame*. 2008; 153:394–416.
16. Jones WP, Prasad VN. Large Eddy simulation of the Sandia Flame Series (D–F) using the Eulerian stochastic field method. *Combust Flame*. 2010;157:1621–1636.
17. Balarac G, Pitsch H, Raman V. Modeling of the subfilter scalar dissipation rate using the concept of optimal estimators. *Phys Fluids*. 2008;20:091701.
18. Balarac G, Pitsch H, Raman V. Development of a dynamic model for the subfilter scalar variance using the concept of optimal estimators. *Phys Fluids*. 2008;20:035114.
19. Kaul CM, Raman V, Balarac G, Pitsch H. Numerical errors in the computation of subfilter scalar variance in large eddy simulations. *Phys Fluids*. 2009;21:055102.
20. Komori S, Kanzaki T, Murakami Y, Ueda H. Simultaneous measurements of instantaneous concentrations of two species being mixed in a turbulent flow by using a combined laser-induced fluorescence and laser-scattering technique. *Phys Fluids A*. 1989;1:349–352.
21. Komori S, Hunt JCR, Kanzaki T, Murakami Y. The effects of turbulent mixing on the correlation between two species and on concentration fluctuation in non-premixed reacting flow. *J Fluid Mech*. 1991;228:629–659.
22. Komori S, Nagata N, Kanzaki T, Murakami Y. Measurements of mass flux in a turbulent liquid flow with a chemical reaction. *AIChE J*. 1993;39:1611–1620.
23. Komori S, Kanzaki T, Murakami Y. Concentration correlation in a turbulent mixing layer with chemical reactions. *J Chem Eng Jpn*. 1994;27:742–748.
24. Cook AW. Determination of the constant coefficient in scale similarity models of turbulence. *Phys Fluids*. 1997;9:1485–1487.
25. Christopher TC, Stephan CJ, Ramsey JM. Diffusion coefficient measurements in microfluidic devices. *Talanta*. 2002;56:365–373.
26. Suriani AR, Betsay P, Philip SS. Rapid diffusion of fluorescent tracers into *Staphylococcus epidermidis* biofilms visualized by time lapse microscopy. *Antimicrob Agents Chemother*. 2005;49:728–732.
27. Batchelor GK. Small-scale variation of convected quantities like temperature in turbulent fluid. Part 1. General discussion and the case of small conductivity. *J Fluid Mech*. 1959;5:113–133.
28. Hinze JO. *Turbulence*, 2nd ed. New York: McGraw-Hill, 1975.
29. Wang Y, Tanahashi M, Miyauchi T. Coherent fine scale eddies in turbulence transition of spatially-developing mixing layer. *Int J Heat Fluid Flow*. 2007;28:1280–1290.
30. Liu Y, Fox RO. CFD predictions for chemical processing in a confined impinging-jets reactor. *AIChE J*. 2006;52:731–744.
31. Bradley N, Jones WP. Large eddy simulation of turbulent non-premixed flame. In Proceedings of the Eleventh Symposium on Turbulent Shear Flows, Grenoble, France, 1997;4.1–4.6.
32. Bradley N, Jones WP. *Large eddy simulation of a nonpremixed turbulent swirling flame*. In: Rodi W, Laurence D, editors. *Engineering Turbulence Modelling and Experiments 4*. Amsterdam: Elsevier Science, 1999:861–870.
33. Cook AW, Bushe WK. A subgrid-scale model for the scalar dissipation rate in nonpremixed combustion. *Phys Fluids*. 1999;11:746–748.

Manuscript received Jun. 15, 2010, and revision received Jan. 13, 2011.